Dispersive coupled-channel analysis of nucleon scattering from ^{232}Th up to 200 MeV

E. Sh. Soukhovitskii
Joint Institute for Energy and Nuclear Research, 220109, Minsk-Sosny, Belarus

R. Capote*
Nuclear Data Section, International Atomic Energy Agency, Wagramerstrasse 5, Vienna A-1400, Austria

J. M. Quesada
Departamento de Física Atómica, Molecular y Nuclear, Universidad de Sevilla, Ap.1065, E-41080 Sevilla, Spain

S. Chiba
Advanced Science Research Center, Japan Atomic Energy Research Institute, Tokai, Naka, Ibaraki 319-1195, Japan
(Received 14 March 2005; published 11 August 2005)

An isospin-dependent coupled-channels optical model potential containing a dispersive term (including nonlocal contribution) is used to simultaneously fit the available experimental database (including strength functions and scattering radius) for neutron and proton scattering on strongly deformed ^{232}Th nucleus. The energy range 0.001–200 MeV is covered. A dispersive coupled-channel optical model potential with parameters that show a smooth energy dependence and energy independent geometry are determined from fits to the entire data set. Dispersive contribution is shown to be the dominant Coulomb correction to the proton real potential below the Coulomb barrier. Inclusion of nonlocality effects in the absorptive volume potential and its corresponding dispersive contribution to the real potential is needed to achieve an excellent agreement above 100 MeV.

DOI: 10.1103/PhysRevC.72.024604 PACS number(s): 11.55.Fv, 24.10.Ht, 24.10.Eq, 25.40.−h

I. INTRODUCTION

During the past 50 years the nuclear optical model has been extensively applied to analyze the elastic scattering of pions, nucleons, and heavier particles by nuclei over a wide range of energies [1–3]. It has been extended to include inelastic scattering by the coupled-channels formalism [4,5] and consideration of dispersion effects allows us to describe both bound and scattering states by the same nuclear mean field [6–16]. These dispersion effects follow from the requirement of causality, namely that the scattering wave is not emitted before the incident wave arrives [7]. In this way a physically self-consistent description of the energy dependence of the optical model potential is obtained. Moreover, additional constraint imposed by dispersion relations helps to reduce the ambiguities in deriving phenomenological optical model potential (OMP) parameters from the experimental data.

Pioneering works on dispersive optical model (DOM) analysis for nucleon scattering have been done by Lipperheide [17,18], Passatore [19], and Lipperheide and Schmidt [20]. A great success has been achieved in deriving DOM potentials for nucleon scattering on closed shell nuclei such as ^{40}Ca,^{90}Zr, and ^{208}Pb. Many studies have dealt also with neutron scattering on near to magic nuclei. A global spherical potential for nucleon-induced reactions derived by Koning and Delaroche [21] used local dispersive OMPs as starting point [22]. Recently a global dispersive spherical potential for neutron-induced reactions was derived by Morillon and Romain [23]. However, very few studies have been devoted to DOM potentials for strongly deformed nuclei, where coupled-channel formalism should include dynamical potential corrections arising from dispersion effects. The first work on this subject was, to our knowledge, the contribution of Romain and Delaroche [24], which was devoted to the analysis of the nucleon scattering data on ^{181}Ta and tungsten isotopes. An explicit treatment of the nonlocality of the surface imaginary potential (symmetric about the Fermi energy E_F) was used to achieve excellent agreement with Los Alamos–Ohio University experimental data up to 200 MeV [25]. They found that the effect of including the nonlocality in the calculations was the weakening of the dispersive contribution as the energy increases. However, in an earlier contribution from Mahaux and Sartor [15], they pointed out that because of nonlocality effects, the absorptive potential will be highly asymmetric (with respect to E_F). The DOM analysis of neutron scattering on ^{27}Al [26] showed the importance of the dispersive contribution to describe σ_T data for energies above 100 MeV using a nonsymmetric version of the volume absorptive potential for large positive and large negative energies. We present strong evidence to favor nonsymmetric volume absorptive potential for a proper description of the nucleon scattering data for energies above 100 MeV on deformed targets.

Recent studies on gadolinium, hafnium, and holmium isotopes [27–29] also consider dispersive coupled-channel description using symmetric imaginary potentials, but no clear advantage of dispersive against conventional coupled-channel approach was shown, probably because the employed experimental database included only data in very limited energy range up to 20 MeV.

*Electronic address: R.CapoteNoy@iaea.org

Additional motivation for our work is that thorium is an important fissile material for the accelerator-driven system (ADS). Moreover, there is rising interest in innovative fuel cycle concepts based on thorium fuel [30]. Knowledge of accurate cross sections of a number of reactions (e.g., total, elastic and inelastic scattering, capture, and fission) between neutrons and actinides is crucially important for design of various reactor systems. In the ADS of radioactive-waste transmutation and energy generation, the nuclear reaction data are needed both for neutrons and protons as projectiles up to several hundred mega-electron-volts. Optimization of accelerator-driven minor actinide transmutation strategy requests evaluation of cross sections of a large number of actinide nuclides up to ~200 MeV, above which calculations with Monte Carlo cascade-model based codes can be applied. Below this energy, the coupled-channel calculation is required for actinides, which are highly deformed. Using the optical model, one can calculate not only total, elastic, and reaction cross sections but also transmission coefficients needed in the statistical and preequilibrium model calculations. Thus, the OMP parameters that can reproduce well nucleon scattering data over a wide energy range are essential to make reliable nuclear data prediction.

The main purpose of this contribution is to construct a deformed complex mean field felt by neutrons and protons in ^{232}Th theoretically valid from the Fermi energy up to 200 MeV. We follow the "dispersive optical model analysis" [13,14,31], where the unknown potential parameters are derived by performing optical-model fits to experimental scattering cross sections that need to be available over an energy range as broad as possible. The real and imaginary parts of the mean field are connected by a dispersion relation and, moreover, the mean field is required to closely reproduce the experimental value of the Fermi energy E_F for both neutrons and protons. The Lane model [32,33], which assumes isospin symmetry in nuclei, is employed so our nucleon-nucleus OMP can be decomposed into isoscalar and isovector parts.

Recent measurements of the neutron total cross sections for ^{232}Th at energies from 5 MeV up to 560 MeV were published by a Livermore–Los Alamos–Ohio University collaboration [34]. Average total cross section data in the unresolved resonance region were derived by IRMM's group in 2004 [35]. These high-precision data together with earlier nucleon scattering angular distributions and low-energy observables (strength functions and scattering radius) are the database considered at positive energies. The Fermi energy values derived from nuclear masses are used to constrain the mean field value at negative energies. Therefore the energy variation of the model parameters is reasonably defined over a wide range, an extremely important point for a successful dispersive analysis. Because the employed database extends up to 200 MeV and because the recent high-energy σ_T data are very accurate [34] (i.e., the uncertainty $\Delta\sigma_T$ is about $\pm 1\%$), we use relativistic corrections in all our calculations.

There exist nondispersive coupled-channel OMPs describing nucleon scattering on thorium up to high incident energy. Most of the CC potentials suggested for actinides are based on the potentials determined by Lagrange [36]. A new global parametrization using nondispersive CC OMP for actinide nuclei valid from 1keV to 200 MeV was recently proposed by Soukhovitskii and coworkers [37] (in the following we refer to this work as NDOMP04). During the past year, several new OMPs are being discussed in the framework of the ongoing IAEA Coordinated Research Program [30].

The article is structured as follows. Section II provides a description of the coupled-channel dispersive optical model formalism and the forms of the energy and radial dependencies of the real, imaginary and spin-orbit potentials. Section III describes the ^{232}Th experimental scattering database and the resulting isospin dependent potential for the simultaneous description of neutron and proton induced reactions on thorium. In the same section we compare derived DCCOM potential with state-of the-art nondispersive potential [37] and experimental data. Finally Sec. IV contains our conclusions.

II. COUPLED-CHANNEL DISPERSIVE OPTICAL MODEL FORMALISM

A. Optical-model potential

Thorium is a well-deformed rigid rotor, where low-lying collective levels are strongly excited in nucleon inelastic scattering. The customary coupled-channels calculations were performed by coupling the first five states of the ground state $K^\pi = 0^+$ rotational band, $J^\pi = 0^+, 2^+, 4^+, 6^+$, and 8^+. This coupling scheme is denoted as the "saturated coupling" [38]. It means that inclusion of additional levels changes the calculated results within the experimental errors. One must be aware that the experimental data may be described with a coupling of fewer levels. However, optical potential parameters in such a case depend on the coupling scheme used to compensate a lack of coupling strengths. Therefore such optical potential parameters cannot guarantee reliable prediction when they are used with any other coupling schemes or to neighboring actinide nuclei whose experimental data is not available. Our analysis spans an energy range from 0.001 to 200 MeV. Both direct and statistical processes contribute to nucleon-nucleus elastic scattering at these energies. However, according to our estimation, the statistical processes are not important above 3 MeV so we neglect them in the OMP derivation. The direct processes, increasingly dominant at higher energies, can be described by the optical model.

The deformed nuclear optical potential arises from deformed instant nuclear shapes

$$R_i(\theta', \varphi') = R_i^0 \left\{ 1 + \sum_{\lambda=2,4,6,8} \beta_{\lambda 0} Y_{\lambda 0}(\theta', \varphi') \right\}, \quad i = v, s, \mathrm{so}, c, \tag{1}$$

where $Y_{\lambda 0}$ is spherical harmonics; θ' and φ' are angular coordinates in the body-fixed system; v, s, so, and c are volume, surface, spin-orbit, and Coulomb terms; and $R_i^0 = r_i A^{1/3}$, with A being the target mass number.

The optical model potential is taken to be a standard Woods-Saxon form but with account of the deformed nuclear shapes.

It may be written as follows:

$$\begin{aligned} V(r, R(\theta', \varphi'), E) = &- \left[V_v(E) + i W_v(E) + \Delta V_v^{\mathrm{Coul}}(E)\right] \\ &\times f_{\mathrm{WS}}[r, R_v(\theta', \varphi')] - \left[V_s(E) + i W_s(E) \right. \\ &\left. + \Delta V_s^{\mathrm{Coul}}(E)\right] g_{\mathrm{WS}}[\mathbf{r}, R_s(\theta', \varphi')] \\ &- \left(\frac{\hbar}{m_\pi c}\right)^2 [V_{\mathrm{so}}(E) + i W_{\mathrm{so}}(E)] \\ &\times \frac{1}{r}\frac{d}{dr} f_{\mathrm{WS}}[r, R_{\mathrm{so}}(\theta', \varphi')](\hat{\sigma} \cdot \hat{L}) \\ &+ V_{\mathrm{Coul}}[r, R_c(\theta', \varphi')], \end{aligned} \tag{2}$$

where the successive complex-valued terms are the volume, surface, and spin-orbit potentials with the form factors given as follows:

$$\begin{aligned} &f_{\mathrm{WS}}[r, R_i(\theta', \varphi')] \\ &\quad = \{1 + \exp[r - R_i(\theta', \varphi')]/a_i\}^{-1}, \qquad i = v, \mathrm{so} \\ &g_{\mathrm{WS}}[r, R_s(\theta', \varphi')] = -4a_s \frac{d}{dr} f[r, R_s(\theta', \varphi')] \end{aligned} \tag{3}$$

and deformed radii R_i as described in Eq. (1). The Coulomb potential $V_{\mathrm{Coul}}[r, R_c(\theta', \varphi')]$ was calculated using a multipole expansion of charged ellipsoid with a uniform charge density within the Coulomb radius R_c and zero outside as suggested by Satchler *et al*. [39]. The spherical term of the Coulomb potential was calculated by taking account of the diffuseness of the charge density distribution of the form $f_c = [1 + \exp(r - R_c^0)/a_c]^{-1}$ [40].

The Coulomb correction volume $\Delta V_v^{\mathrm{Coul}}(E)$ and surface $\Delta V_s^{\mathrm{Coul}}(E)$ terms are set to have an energy dependence that is a minus derivative of the real potential, so that

$$\Delta V_{v,s}^{\mathrm{Coul}}(E) = -C_{\mathrm{Coul}} \frac{Z Z' e^2}{A^{1/3}} \frac{d}{dE}[V_{v,s}(E)], \tag{4}$$

where the symbols Z' and Z denote charges of projectile and target in electron charge units.

In our formulation of the OMP in Eq. (2) the real and imaginary volume terms share the same geometry parameters r_v and a_v and likewise the real and imaginary surface (spin-orbit) terms share the same $r_s(r_{\mathrm{so}})$ and $a_s(a_{\mathrm{so}})$ parameters. This assumption [9] can be seen as a consequence of the dispersive relations, allowing us to reduce the number of geometrical parameters in the OMP.

As energy losses because of collective levels excitation compared with the nucleon incident energies for low incident energies involved in the analysis are noticeable, the dependence of the local optical potential for different channels was taken into account as follows:

$$V_{if} = V\left(E_p - \frac{E_i + E_f}{2}\right), \tag{5}$$

where i and f denote initial and final channels, whereas E_i and E_f the corresponding level energies.

The present optical potential includes relativistic corrections as discussed by Elton [41]. First, the nucleon wave number k was calculated in the relativistic form:

$$(\hbar k)^2 = [E^2 - (M_p c^2)^2]/c^2 \tag{6}$$

where E denotes the total energy of projectile, M_p the projectile rest mass, and c the velocity of light. Second, projectile and target masses were replaced by corresponding relativistic energies in reduced mass formulae.

In a dispersion relation treatment, the real potential strength consists of a term that varies slowly with energy, the so-called Hartree-Fock (HF) term, $V_{\mathrm{HF}}(\mathbf{r}, E)$, plus a correction term, $\Delta V(\mathbf{r}, E)$, which is calculated using a dispersion relation. Under favorable conditions of analiticity in the complex E-plane the real part ΔV can be constructed from the knowledge of the imaginary part W on the real axis through the dispersion relation

$$\Delta V(\mathbf{r}, E) = \frac{\mathcal{P}}{\pi} \int_{-\infty}^{\infty} \frac{W(\mathbf{r}, E')}{E' - E} dE', \tag{7}$$

where we have now explicitely indicated the radial and energy dependence of these quantities and $\mathcal{P}$ means that the principal value of the integral should be taken. Assuming that $\Delta V(\mathbf{r}, E = E_F) = 0$, where E_F is the Fermi energy, Eq. (7) can also be written in the subtracted form

$$\Delta V(\mathbf{r}, E) = \frac{\mathcal{P}}{\pi} \int_{-\infty}^{\infty} W(\mathbf{r}, E') \left(\frac{1}{E' - E} - \frac{1}{E' - E_F}\right) dE'. \tag{8a}$$

Here E_F denotes the Fermi energy, determined as $E_F(Z, A) = -\frac{1}{2}[S_n(Z, A) + S_n(Z, A + 1)]$ for neutrons and $E_F(Z, A) = -\frac{1}{2}\left[S_p(Z, A) + S_p(Z + 1, A + 1)\right]$ for protons, where $S_i(Z, A)$ denotes the separation energy of nucleon i from a nucleus labeled by Z and A.

For energy-dependent geometry we should use Eq. (8a) directly to calculate the dispersive contribution to the real potential. To simplify the problem, however, the geometry of the imaginary terms of the OMP are usually assumed to be energy independent and they are expressed in terms of a Woods-Saxon function $f_{\mathrm{WS}}(r)$ or its derivative. In such case the radial functions factorize out of the integrals and the energy dependence is completely accounted for by two overall multiplicative strenghts $\Delta V(E)$ and $W(E)$. Both of these factors contain, we note, volume and surface contributions. Using the definitions of Eq. (2), the real volume $V_v(E)$ and surface $V_s(E)$ parts of the dispersive OMP are given by the following:

$$\begin{aligned} V_v(E) &= V_{\mathrm{HF}}(E) + \triangle V_v(E) \\ V_s(E) &= \triangle V_s(E). \end{aligned} \tag{9}$$

It should be noted that the general definition of the Coulomb correction (4) implies the existence of the dynamical dispersive Coulomb correction arising from the derivative of the dispersive contributions $\triangle V_v(E)$ and $\triangle V_s(E)$. To our knowledge such corrections never were discussed before. These dynamical contributions to the Coulomb corrections are the dominant contribution below 20 MeV to the total Coulomb correction to the real potential as discussed later.

It is known that the energy dependence of the depth $V_{\mathrm{HF}}(E)$ is because of the replacement of a microscopic nonlocal HF potential by a local equivalent. For a Gaussian nonlocality $V_{\mathrm{HF}}(E)$ is a linear function of E for large negative E and is an exponential for large positive E. Following Mahaux and Sartor [15], the energy dependence of the Hartree-Fock part of the

nuclear mean field is taken as that found by Lipperheide [18]:

$$V_{\rm HF}(E) = A_{\rm HF}\exp[-\lambda_{\rm HF}(E - E_F)], \tag{10}$$

where the parameters $A_{\rm HF}$ and $\lambda_{\rm HF}$ are undetermined constants. Equation (10) can be used to describe HF potential in the scattering regime [15].

It is useful to represent the variation of surface $W_s(E)$ and volume absorption potential $W_v(E)$ depth with energy in functional forms suitable for the dispersive optical model analysis. An energy dependence for the imaginary volume term has been suggested in studies of nuclear matter theory by Brown and Rho [42]:

$$W_v(E) = A_v\frac{(E - E_F)^2}{(E - E_F)^2 + (B_v)^2}, \tag{11}$$

where A_v and B_v are undetermined constants. An energy dependence for the imaginary-surface term has been suggested by Delaroche *et al*. [13] to be as follows:

$$W_s(E) = A_s\frac{(E - E_F)^2}{(E - E_F)^2 + (B_s)^2}\exp(-C_s|E - E_F|), \tag{12}$$

where A_s, B_s, and C_s are undetermined constants.

The isospin dependence of the potential (the Lane term [32,33]) was considered in real $V_{\rm HF}(E)$ and imaginary surface $W_s(E)$ potentials as follows:

$$A_{\rm HF} = V_0\left[1 + (-1)^{Z'+1}\frac{C_{\rm viso}}{V_0}\frac{N - Z}{A}\right] \tag{13}$$

$$A_s = W_0\left[1 + (-1)^{Z'+1}\frac{C_{\rm wiso}}{W_0}\frac{N - Z}{A}\right], \tag{14}$$

where V_0, $C_{\rm viso}$, W_0, and $C_{\rm wiso}$ are undetermined constants.

The symmetry condition

$$W(2E_F - E) = W(E) \tag{15}$$

is used to define imaginary part of the OMP for energies below the Fermi energy.

B. High-energy behavior of the volume absorption

The assumption that the imaginary potential $W_v(E)$ is symmetric about $E' = E_F$ [according to Eq. (15)] is plausible for small values of $|E' - E_F|$; however, as was pointed out by Mahaux and Sartor [15], this approximate symmetry no longer holds for large values of $|E' - E_F|$. In fact the influence of the nonlocality of the imaginary part of the microscopic mean field will produce an increase of the empirical imaginary part $W(r, E')$ at large positive E' and approaches zero at large negative E' [6,43]. Following Mahaux and Sartor [15], we assume that the absorption strengths are only modified above some fixed energy E_a. They used $E_a = 60$ MeV; however, this value is fairly arbitrary [15] and we use it as a fitting parameter. Let us assume the nonlocal imaginary potential to be used in the dispersive integral is denoted by $\widetilde{W}_v(E)$. We can then write [16]

$$\widetilde{W}_v(E) = W_v(E) - W_v(E) \times\frac{(E_F - E - E_a)^2}{(E_F - E - E_a)^2 + E_a^2}, \quad \text{for } E < E_F - E_a \tag{16}$$

and

$$\widetilde{W}_v(E) = W_v(E) + \alpha\left[\sqrt{E} + \frac{(E_F + E_a)^{3/2}}{2E} - \frac{3}{2}\sqrt{(E_F + E_a)}\right], \quad \text{for } E > E_F + E_a. \tag{17}$$

These functional forms are chosen in such a way that the function and its first derivative are continuous at $E' = |E_F - E_a|$. At large positive energies nucleons sense the "hard core" repulsive region of the nucleon-nucleon interaction and $\widetilde{W}_v(E)$ diverges like $\alpha\sqrt{E}$. Using a model of a dilute Fermi gas hard-sphere the coefficient α can be estimated to be equal to 1.65 MeV$^{1/2}$ [43], assuming that the Fermi impulse k_F is equal to 1.36 fm^{-1}and the radius of the repulsive hard core is equal to 0.4 fm. On the contrary, at large negative energies the volume absorption decreases and goes asymptotically to zero.

The asymmetric form of the volume imaginary potential of Eqs. (16) and (17) results in a dispersion relation that must be calculated directly from Eq. (8a) and separates into three additive terms [44]. Therefore, we write the dispersive volume correction in the following form:

$$\triangle\widetilde{V}_v(E) = \triangle V_v(E) + \triangle V_<(E) + \triangle V_>(E), \tag{18}$$

where $\triangle V_v(E)$ is the dispersive correction because of the symmetric imaginary potential of Eq. (11) and the terms $\triangle V_<(E)$ and $\triangle V_>(E)$ are the dispersive corrections because of the asymmetric terms of Eqs. (16) and (17), respectively. Although the symmetric case features an equal contribution coming from negative and positive energies, in the asymmetric case the negative energy contribution to the dispersive integral is very different from the positive energy value. The resulting dispersive correction for the asymmetric case starts to increase already for energies above 50 MeV, making a significant contribution to the real part of the OMP at high energies. It should be noted that nonlocality corrections [Eqs. (16) and (17)] can be used either for the volume or surface imaginary potential; however, Mahaux and Sartor [15] have shown that nonlocality consideration for the surface imaginary potential has a very small effect on the calculated cross sections. Therefore in this work we followed Ref. [16] and considered only the effects of nonlocality in the volume absorption.

C. Spin-orbit potential

For the energy dependence of the spin-orbit potential we started from the functional form suggested by Koning and Delaroche [21], namely:

$$V_{\rm so}(E) = V_{\rm SO}\exp[-\lambda_{\rm so}(E - E_F)] \tag{19}$$

$$W_{\rm so}(E) = W_{\rm SO}\frac{(E - E_F)^2}{(E - E_F)^2 + (B_{\rm so})^2}. \tag{20}$$

In this work we connected the imaginary spin-orbit potential $W_{so}(E)$ to the real spin orbit potential $V_{so}(E)$ by a dispersion relation as discussed by Walter [45] and first carried out by Morillon and Romain [23]. The real spin-orbit potential is calculated as follows:

$$V_{so}(E) = V_{SO} \exp[-\lambda_{so}(E - E_F)] + \Delta V_{so}(E). \quad (21)$$

Spin-orbit functional (20) is exactly the same as the one employed for symmetric volume absorptive potential (11), so the dispersive contribution $\Delta V_{so}(E)$ to the real spin-orbit potential can be calculated using the analytical expressions for volume absorptive potential derived by Quesada *et al*. [46].

III. DISPERSIVE COUPLED-CHANNEL OPTICAL MODEL ANALYSIS

A. Summary of the experimental databases

A survey of the experimental data spanning from 0.001 to 200 MeV used in the DCCOM analyzes is presented in this section. The potential parameters were searched for to reproduce available neutron and proton-induced cross-section data for ^{232}Th. At incident energies above several mega-electron-volts. It is almost impossible to separate neutron inelastic scattering data into each excitation level experimentally for actinide nucleus. Thus experimental proton-scattering data, which can be done with much higher resolution, was highly relevant to determine the optical potential parameters uniquely.

Averaged total neutron cross sections with associated errors for energies from 0.001 up to 5 MeV [47–51] were employed to avoid oscillating behavior of the experimental total cross section. Additional average total cross-section data in the unresolved resonance region from 1 up to 140 keV were recently measured by IRMM's group [35]. Energy-averaged total cross sections σ_T were obtained from Abfalterer *et al*. [34] from 5 to 200 MeV. The total cross section data considered cover all the critical energy points which are necessary to reveal the structure because of the Ramsauer effect. The following experimental scattering data for ^{232}Th were used in the current analysis: neutron-scattering data by Haouat *et al*. for excitation of resolved 0^+, 2^+, and 4^+ levels for energy of 3.4 MeV [52]; neutron-scattering data by Smith and Chiba for excitation of a sum of 0^+, 2^+, 4^+, 6^+, and 8^+ 12 at twelve incident energies from 4.5 to 10.0 MeV [53]; neutron-scattering data by Batchelor *et al*. for excitation of a sum of 0^+, 2^+, 4^+, 6^+, and 8^+ levels at 4 and 7 MeV [54]; neutron-scattering data by Iwasaki *et al*. for excitation of a sum of 0^+, 2^+, and 4^+ levels at 5.7 MeV [55]; neutron-scattering data by Dagge *et al*. for excitation of a sum of 0^+, 2^+, 4^+, 6^+, and 8^+ at 7.75 MeV [56]; neutron-scattering data by Hansen *et al*. [57] and Dukarevich *et al*. [58] for excitation of a sum of 0^+, 2^+, 4^+, 6^+, and 8^+ levels at 14.1 MeV; neutron-scattering data by Hudson *et al*. for excitation of a sum of 0^+, 2^+, 4^+, 6^+, and 8^+ levels at 15.2 MeV [59]; proton-scattering data by Hansen *et al*. for excitation of resolved 0^+, 2^+, 4^+, 6^+, and 8^+ levels at 20 and 26 MeV [60]; proton-scattering data by King *et al*. for excitation of resolved 2^+, 4^+, 6^+, and 8^+ levels at 35 MeV [61]; and proton-scattering data by Takeuchi *et al*. for excitation of resolved 0^+, 2^+, 4^+, and 6^+ levels at 65 MeV [62,63]. It must be noted that the data of Takeuchi *et al*. for the first four levels of ^{232}Th [62], which are very important for fixing cross sections at a high-energy region (this is the only angular distribution measured above 35 MeV with high energy resolution), were erroneously given in EXFOR database. Professor H. Sakaguchi kindly supplied us correct data [63]. Evaluated neutron strength function for ^{232}Th, S_0 and, S_1, and potential scattering radius R' [35,64] were used in parameter search.

For chosen scattering experimental data we assumed that the interaction of nucleons with ^{232}Th proceeds only via the direct mechanism. For this reason, the neutron-scattering data at incident energies below 3.4 MeV were not used in this investigation becuase those data contain a compound contribution that was not considered in the search procedure.

The optical potential parameters were searched for by minimizing the quantity χ^2 defined by the following:

$$\chi^2 = \frac{1}{N+M+3}\left[\sum_{i=0,1}\left(\frac{S_{i,calc} - S_{i,eval}}{\Delta S_{i,eval}}\right)^2 + \left(\frac{R'_{calc} - R'_{eval}}{\Delta R'_{eval}}\right)^2 + \sum_{i=1}^{N}\frac{1}{K_i}\sum_{j=1}^{K_i}\left(\frac{d\sigma_{ij}/d\Omega_{calc} - d\sigma_{ij}/d\Omega_{exp}}{\Delta d\sigma_{ij}/d\Omega_{exp}}\right)^2 + \sum_{i=1}^{M}\left(\frac{\sigma_{tot_{cal_i}} - \sigma_{tot_{eval_i}}}{\Delta\sigma_{tot_{eval_i}}}\right)^2\right], \quad (22)$$

where N denotes number of experimental scattering data sets, K_i the number of angular points in each scattering data set, and M the number of energies for which the experimental (evaluated) neutron total cross section is involved.

B. The ^{232}Th DCCOM analysis

1. Parameter fitting

Optical model code OPTMAN [65,66] was used for OMP parameter fitting. Originally the code did not include dispersion terms, so numerical [67] and analytical solutions [46,68] of dispersion relations were implemented within the OPTMAN code. We were using symmetric surface and nonsymmetric volume imaginary absorptive potentials according to Eq. (12), (16), and (17), therefore we adjusted 14 parameters, namely (V_0, λ_{HF}, C_{viso}), which define the smooth energy dependence of the real volume potential; W_0, C_{wiso}, B_s, C_s and A_v, B_v, E_a defining the surface and volume absorptive potential respectively plus geometrical parameters (r_v, a_v, r_s, a_s). After proper values were obtained by this global minimization spin-orbit parameters V_{so}, λ_{so}, A_{so}, B_{so}, r_{so}, and a_{so}, parameters of the Coulomb interaction, C_{Coul}, r_c, and a_c and multipolar deformation parameters β_i were also optimized. The final iteration involved a free variation of all parameters using the best-fit search option of the OPTMAN code. The derived

TABLE I. Dispersive coupled-channel OMP parameters for ^{232}Th (RIPL OMP index 608 [64]).

	Volume	**Surface**	**Spin-orbit**	**Coulomb**
Real depth (MeV)	$V_0 = 49.97$ $\lambda_{HF} = 0.01004$ $C_{viso} = 15.9$	dispersive	$V_{so} = 5.75$ $\lambda_{so} = 0.005$	$C_{Coul} = 1.3$
Imaginary depth (MeV)	$A_v = 12.04$ $B_v = 81.36$ $E_a = 385$	$W_0 = 17.20$ $B_s = 11.19$ $C_s = 0.01361$ $C_{wiso} = 23.5$	$W_{so} = -3.1$ $B_{so} = 160$	
Geometry (fm)	$r_v = 1.2568$ $a_v = 0.633$	$r_s = 1.1803$ $a_s = 0.601$	$r_{so} = 1.1214$ $a_{so} = 0.59$	$r_c = 1.2452$ $a_c = 0.545$

Note. We used the following deformation parameters of ^{232}Th: $\beta_2 = 0.213$, $\beta_4 = 0.066$, and $\beta_6 = 0.0015$.

DCCOM potential parameters are listed in Table I. The attained minimum χ^2 value, as defined by Eq. (22), for all the available ^{232}Th experimental data is 2.55, being 2.23 for the neutron database, whereas for proton angular data description the corresponding χ^2 minimum is 3.49. These values compared favorably with the NDOMP04 values, which are 2.55 and 3.8 for neutron and proton databases respectively.

2. Fermi energies

We used the DCCOM parameters to calculate the Fermi energies predicted by the extension of our potential to negative energies. The dispersive corrections and all imaginary potentials vanish at the Fermi energy. Therefore, we needed to consider only the real volume potential defined by Eqs. (10) and (13) and the real spin-orbit potential Eq. (19). Additionally, the nondispersive part of the Coulomb correction [Eq. (4)] must be taken into account for the proton potential. Using the parameters from the Table I, we calculated real volume and spin-orbit potential depths at the Fermi energy. The obtained values are 46.41/53.5 MeV for the neutron/proton volume potential, whereas the spin-orbit depth is 5.75 MeV. Additionally, 10.23 MeV coming from the Coulomb correction should be added to the proton potential depth. We employed the shell-model code CASSINI [69] to calculate the single-particle level energies in a neutron/proton potential corresponding to $n + {}^{232}\mathrm{Th}/p + {}^{232}\mathrm{Th}$ system. For the neutron system, we obtained $E_F = -6.3$ MeV, whereas for the proton system $E_F = -9.0$ MeV. These values should be compared with the experimental Fermi energies of -5.61 and -6.50 MeV respectively. Given the uncertainty in the real potential depth and limitations of the available data, we consider the agreement to be satisfactory, specially for the neutron channel. It should be stressed that proton potential is strongly influenced by a Coulomb correction. A 20% change in the Coulomb correction is enough to bring the proton Fermi energy within 1 MeV of the experimental value. Unfortunately, the lack of proton measurements near and below the Coulomb barrier makes very difficult a precise estimation of the Coulomb correction.

3. Comparison with experimental databases

The total neutron cross-section data for ^{232}Th in the energy region from 0.001 up to 200 MeV is compared against selected experimental data [34,35,49–51] in Fig. 1. The measurements are excellently reproduced by the axial rigid-rotor DCCOM calculations with the present optical potential parameters from Table I. The coupled-channel model makes it possible to calculate also the angular distributions for scattering of neutrons and protons to the low-lying collective levels of ^{232}Th. Elastic and inelastic experimental neutron- and proton-scattering data are described fairly well with the DCCOM calculations as can be seen in Figs. 2 and 3. Furthermore, calculated average resonance parameters reproduce the evaluated values very well, as shown in Table II. It is important to remark the advantage of dispersive approach for average resonance parameters description. The

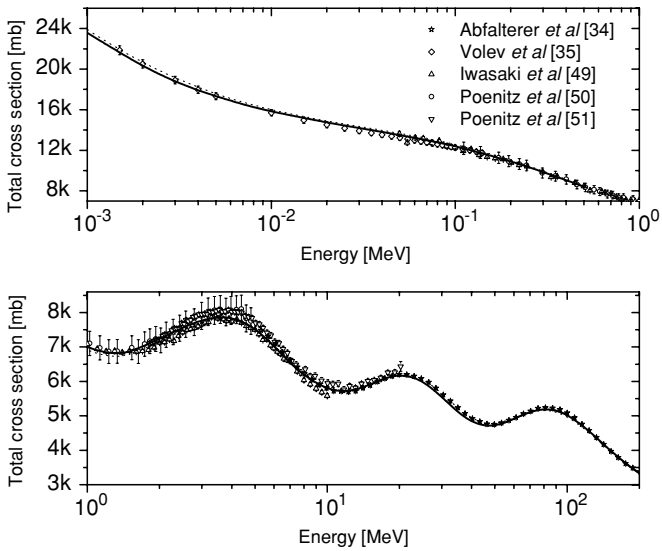

FIG. 1. Neutron total cross sections for ^{232}Th for energies 0.001 to 1 MeV (top panel) and 1 to 200 MeV (bottom panel). Solid lines are the result of present calculations, whereas dotted lines correspond to the nondispersive OMP of Ref. [37]. Experimental data are shown by various symbols.

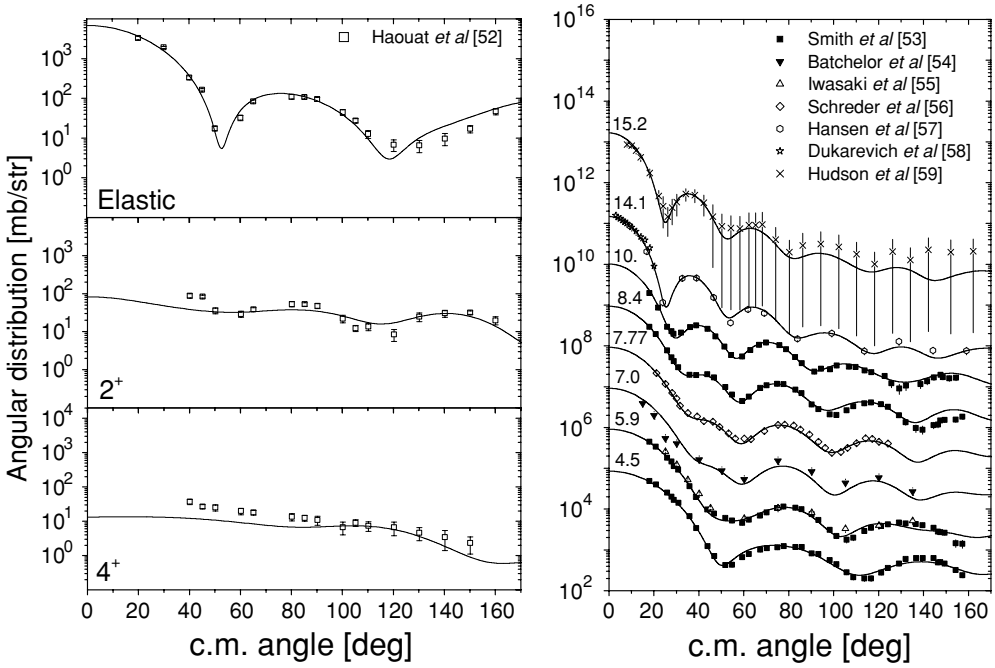

FIG. 2. Selected neutron scattering cross sections on ^{232}Th in center of mass (c.m.) system. Solid lines are the result of present calculations. Experimental data are shown by various symbols. The scattering cross sections to the resolved 0^+, 2^+, and 4^+ levels of ^{232}Th at 3.4 MeV are shown in the left column. The scattering cross sections for excitation of a sum of 0^+, 2^+, 4^+, 6^+, and 8^+ levels of ^{232}Th from 4.5 to 15.2 MeV are shown in the right column. Incident energy for plots appearing on the right pannel is indicated by a number on top of each plot.

real potential of this work is almost flat toward the low energies, by a combination of the increasing contribution of the smooth "Hartree-Fock" $V_{\rm HF}(E)$ potential with the decreasing dispersive contribution (which goes to zero at Fermi energy). Such behavior allows for a good simultaneous description of the average low-energy total cross sections, strength functions, and scattering radius. This simultaneous description is a tough challenge for conventional non-dispersive potentials. The proton nonelastic cross section, $\sigma_{\rm p,non}$, can be compared favorably with experimental data [70,71], Varashenkov's systematic [72], and NDOMP04 results, as can be seen in Fig. 4. It should be noted that proton nonelastic cross section was not included in the fitting process, so its description validates the derived potential and, specially, its isospin dependence. Analysis of the ^{232}Th(p,n) process could be useful for further testing of the isovector component of the DCCOM potential and its Lane's consistency, but it is out of the scope of the present work.

The derived optical potential energy dependence is very simple. We do not need to introduce energy-dependent geometry and the potential parameters are unique for both neutron and proton projectiles. The dispersion relations, coupled to the smooth energy-dependent Hartree Fock potential $V_{\rm HF}(E)$, fully determine the real part of the dispersive contribution once the imaginary part of the mean field is fixed. Very few parameters are required in comparison with a conventional nondispersive coupled-channel OMP analysis (like NDOMP04). The methodology presented here allows to derive similar dispersive coupled-channel optical model of other actinides, This study is ongoing and will be presented elsewhere.

4. Effective mass

The real-potential energy dependence is related to the effective mass m^* through the expression

$$\frac{m^*}{m} = 1 - \frac{d}{dE}[V_r(E)] \tag{23}$$

The effective mass, m^*, can be compared with values deduced from the nonlocality of the nuclear forces [28], as discussed, for example, by Brueckner *et al*. [73] and Perey and Buck [74]. It is shown by Brown *et al*. [75] and Mahaux and Ngo [76] that well away from the Fermi energy the ratio $m^*/m \cong 0.68$, which is reasonably consistent with nuclear matter estimates [77,78]. The derivative in energy of the real-volume part (including the volume dispersive contribution) of the proposed neutron OMP is almost constant below 10 MeV and equal 0.26, which implies a ratio m^*/m˜0.74, a litle higher than theoretical estimates. However, we should keep in mind that the derivative of the real-surface potential, being purely dispersive in nature, changes rapidly in the same energy region from 0.2 up to -0.25. Given the uncertainty and limitations of the available data, the derived potential seems to be in good agreement with these theoretical concepts.

5. Volume Integrals

The spherical volume integrals per nucleon of the real J_V/A and imaginary J_W/A parts of the optical potential were determined for DCCOM and NDOMP04 parameters and are displayed in Fig. 5. The volume and surface contributions are also shown. The inset shows the low-energy dependence of the neutron real volume integral, which is proportional

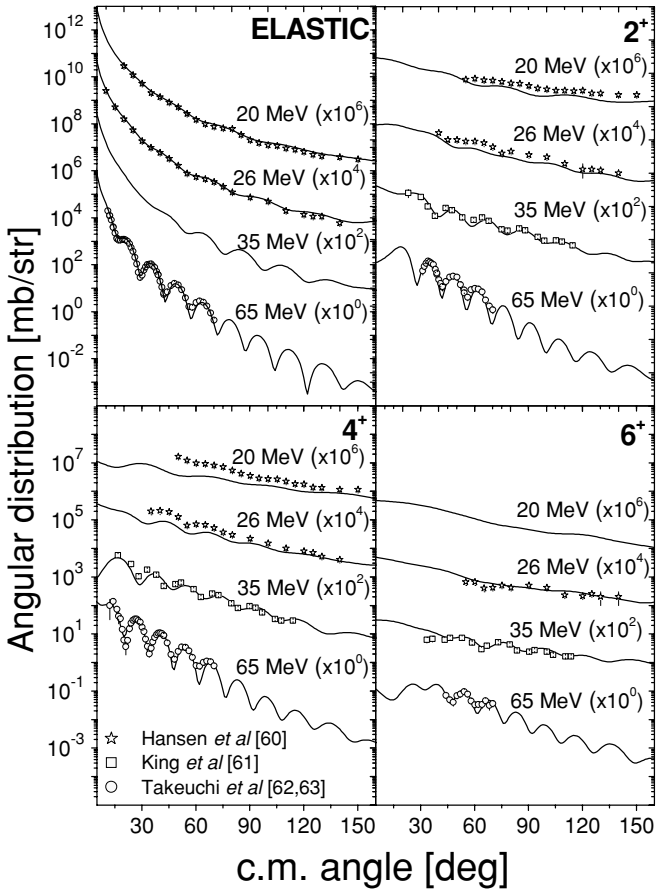

FIG. 3. Selected proton scattering cross sections on ^{232}Th from 20 to 65 MeV in c.m. system. Solid lines are the result of present calculations. Experimental data are shown by various symbols. The corresponding excited level of the Th^{232} rotational band is indicated in the top right corner of each pannel (*ELASTIC* corresponds to the 0^+ ground state). Incident energy is indicated by a number on top of each plot.

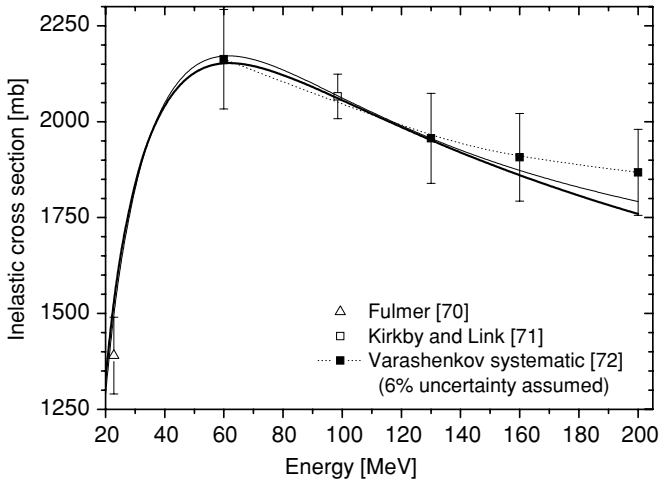

FIG. 4. Reaction cross section for protons incident on ^{232}Th. Solid bold line is the result of present calculations, whereas thin line corresponds to the nondispersive OMP of Ref. [37]. Experimental data are shown by various symbols. Barashenkov systematic [72] is represented by dotted line (systematic is given for U^{238} reaction cross section, which was corrected by the $0.9832 = 232^{1/3}/238^{1/3}$ ratio). Uncertainty of 6% was assumed, equal to the difference between total cross section measured by Abfalterer *et al*. [34] and predicted by systematic [72].

to the cube of the effective radius of the real potential. The typical behavior of the effective potential radius for dispersive potential is observed for DCC OM curve. The absorption in both neutron and proton channels is slightly decreased in our potential for energies above 100 MeV in comparison with NDOMP04 results. The biggest difference between DCCOM and NDOMP04 real-volume integrals is observed in the proton channel, below 30 MeV, where surface Coulomb correction is quite significant as discussed in the next section. The agreement between real-volume integral calculated by DCCOM and NDOMP04 potentials in the neutron channel is almost perfect. However, such "perfect" agreement, which is because of parameter adjustment to the same experimental database, hides the fact that the real-volume integral of our potential is largely determined by dispersive contributions. In fact, we represented in Fig. 6 the contribution of different components in percentage of the real-volume integral both for neutron and proton projectiles, namely

(i) the full dispersive contribution to the real-volume integral
(ii) the dispersive volume contribution to the real-volume integral $J_{\Delta\widetilde{V}_v(E)}/J_V(E)$ and its nonsymmetric part, $J_{\Delta V_< + \Delta V_>}/J_V(E)$
(iii) the dispersive surface contribution to the real-volume integral $J_{\Delta V_s}/J_V(E)$
(iv) the volume $J_{\Delta V_v^{\mathrm{Coul}}}/J_V(E)$ and surface $J_{\Delta V_s^{\mathrm{Coul}}}/J_V(E)$ Coulomb correction's contributions to the real-volume integral for protons

We can observe that dispersive effects contribute to more than 40% of the real-volume integral already at 100 MeV. However the surface and volume dispersive contributions are of different sign, so the overall effect is reduced to about 13% for protons and about 20% for neutrons at 100 MeV. These values reach almost 40 and 50% at 200 MeV for protons and neutrons respectively. It is interesting that the

TABLE II. Comparison of predicted resonance parameters with experimental ones.

Present work (evaluated at 2 keV)			Evaluated values		
$S_0, (eV)^{-1/2}10^{-4}$	$S_1, (eV)^{-1/2}10^{-4}$	R', fm	$S_0, (eV)^{-1/2}10^{-4}$	$S_1, (eV)^{-1/2}10^{-4}$	R', fm
0.868	1.91	9.588 (at 10 keV)	0.94 (0.05) [35] 0.87 (0.07) [64]	1.83 (0.02) [35]	9.52 (0.2) [35] (at 10 keV)

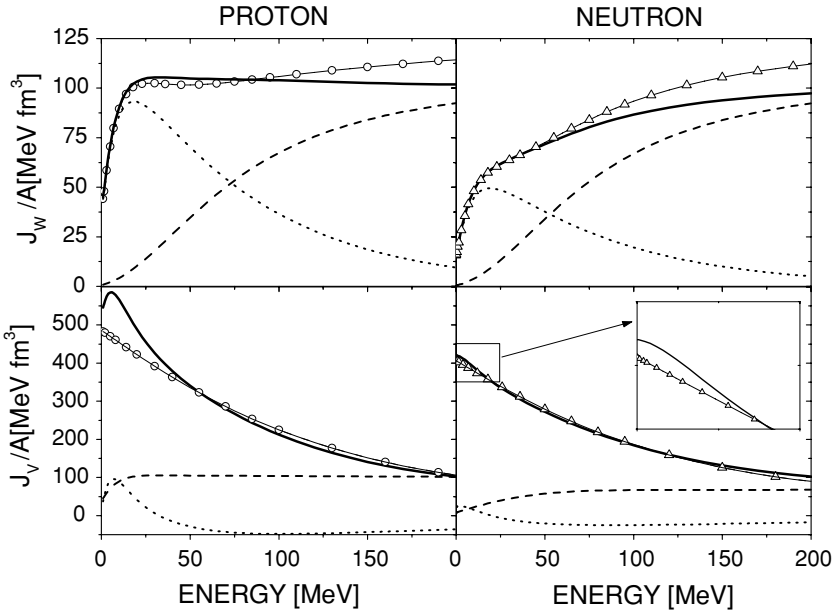

FIG. 5. Energy dependence of the average volume integrals per nucleon of the imaginary (top) and real (bottom) components of the mean field both for protons (left) and neutrons (right). Bold lines correspond to present calculations, whereas empty circles for protons and triangles for neutrons correspond to the nondispersive OMP of Ref. [37]. The volume (dashed) and surface (dotted) contributions to the imaginary volume integral for the present DCC OMP are shown for protons and neutrons in the top panels. The volume (dashed) and surface (dotted) dispersive contributions to the real volume integral are shown in the bottom panel. Expanded low-energy region of the real neutron volume integral is included in the inset.

dispersive contribution itself is dominated at high energies by the contribution coming from the nonsymmetric imaginary volume potential as a result of the nonlocality. In addition, there is an increase of the dispersive correction's contribution below 50 MeV, related to the surface dispersive contribution. Around 30 MeV the surface dispersive contribution reachs a minimum and then changes the sign, becoming positive. This pure dispersive effect cannot be simulated by any variation of nondispersive OMP parameters.

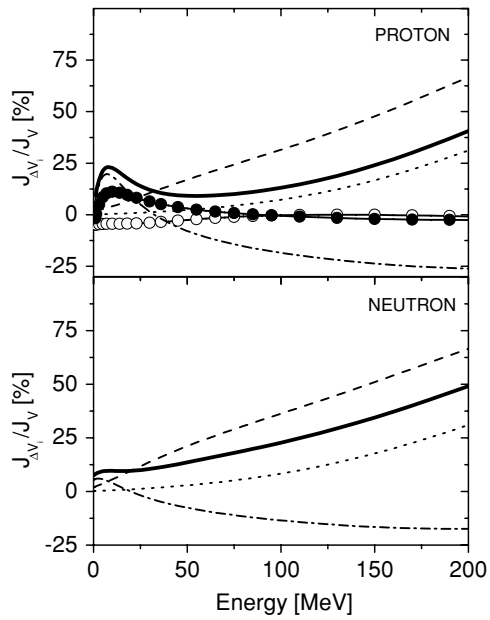

FIG. 6. Energy dependence of partial contributions (in percentages) of the dispersive potentials to the real-volume integral per nucleon $J_V(E)/A$ for the proton (top) and neutron (bottom) DCCOM potential of this work. Solid lines correspond to the full dispersive contribution in each panel. The volume-dispersive contribution $J_{\Delta\tilde{V}_v(E)}/J_V\,(E)$ is shown by a dashed line and the asymmetric part $J_{\Delta V_< + \Delta V_>}/J_V\,(E)$ by dotted line. The dispersive surface contribution to the real-volume integral $J_{\Delta V_s}/J_V\,(E)$ is displayed with a dot-dashed line. The volume $J_{\Delta V_v^{\rm Coul}}/J_V\,(E)$ (open circles) and surface $J_{\Delta V_s^{\rm Coul}}/J_V\,(E)$ (solid circles) Coulomb correction's contributions to the real-volume integral for protons, including dispersive Coulomb correction, are also shown in the upper panel.

6. Coulomb correction to the real potential

In the comprehensive study of Koning and Delaroche [21] it was carried out an analysis of the effect of the energy dependent Coulomb correction term $\Delta V_v^{\rm Coul}(E)$ on their OMP predictions. A comparison with the usual constant Coulomb correction term $\Delta V_v^{\rm Coul} = 0.42Z/A^{1/3}$ revealed that the description of proton-scattering data with the constant term was not as satisfactory as it was with the energy dependent Coulomb correction, specially for energies higher than 120 MeV [21]. In Fig. 7 we compare the volume integral of the Coulomb correction derived in this work, with the correction used in NDOMP04. The NDOMP04 Coulomb correction is similar to the one derived by Koning and Delaroche [21]. The volume Coulomb correction $\Delta V_v^{\rm Coul}(E)$ also behaves like the NDOMP04 correction, even if it includes a dispersive Coulomb correction contribution $d/dE[\Delta V_v(E)]$. However, we have an additional contribution to the real Coulomb volume integral coming from the surface dispersive Coulomb correction $d/dE[\Delta V_s(E)]$. We can see that surface dispersive Coulomb correction $\Delta V_s^{\rm Coul}(E)$ is the dominant contribution to the total Coulomb correction below 20 MeV, making the Coulomb correction for our DCCOMP almost 3 times bigger than the NDOMP04 correction around 10 MeV. These big differences between NDOMP04 and DCCOMP Coulomb corrections are not reflected in the calculated proton reaction cross section (see Fig. 4), probably because the maximum effect is located well below the Coulomb barrier. However, the χ^2 obtained for the proton angular data description was 3.49, which can be favorably compared to the NDOMP04 χ^2 of 3.8 (see p. 916 of Ref. [37]). Therefore, the Coulomb correction, as

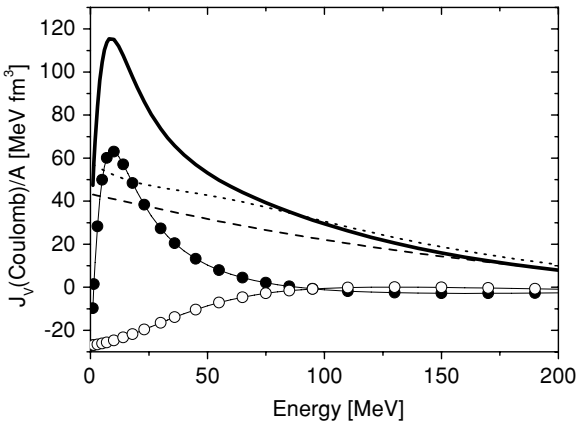

FIG. 7. Energy dependence of the volume integral per nucleon for the Coulomb correction to the real potential calculated for the nondispersive OMP of Ref. [37] (dashed line) and for DCCOM potential (solid line). The volume $J_{\Delta V_v^{\rm Coul}/A}(E)$ (dotted line) and surface $J_{\Delta V_s^{\rm Coul}/A}(E)$ (solid circles) Coulomb correction's contributions to the real-volume integral for protons are also shown. The dispersive volume Coulomb correction, included into $J_{\Delta V_v^{\rm Coul}/A}(E)$, is shown by open circles.

defined by Eq. (4), including dispersive contributions, was important for satisfactory simultaneous fit of neutron- and proton-scattering data. A careful measurement of reaction cross section for proton induced reactions below the Coulomb barrier might provide additional constrains to derive dispersive potentials of the type discussed in this contribution. We would like to point out that dynamical Coulomb correction $d/dE[\Delta V_{v,s}(E)]$ introduced here could be also important in the dispersive optical model description of heavy ion elastic scattering near the Coulomb barrier [7,79,80].

IV. CONCLUSIONS

In this work we have presented a dispersive isospin dependent relativistic coupled-channel optical model analysis of nucleon scattering on ^{232}Th nucleus from 1 keV to 200 MeV. The use of proton and neutron scattering data simultaneously made it possible to increase the accuracy of estimated optical potential parameters especially at high energy region. The isovector terms give the possibility to extend the derived potential parameters to neighboring actinide nuclei. The excellent overall agreement obtained between predictions and experimental data would not have been possible without including dispersive terms in the calculations and nonlocality effects in the volume absorptive potential.

ACKNOWLEDGMENTS

This work was partially supported by International Atomic Energy Agency, by Japan under ISTC Project B-521 and by the European Union under contract FIKW-CT-2000-00107. The authors are grateful to Professor H. Sakaguchi of Kyoto University for supplying us correct proton scattering data at 65 MeV. One of us (RC) is grateful to A. Trkov for encouraging discussions and comments.

[1] P. E. Hodgson, *The Optical Model of Elastic Scattering* (Clarendon Press, Oxford, 1963).
[2] P. E. Hodgson, *Nuclear Reactions and Nuclear Structure* (Oxford University Press, 1971).
[3] P. E. Hodgson, The nuclear optical model: Introductory overview. In *Proceedings of the Meeting on Nucleon-Nucleus Optical Model up to 200 MeV, Bruyères-le-Châtel*, p. 13. Available online at http://www.nea.fr/html/science/om200/
[4] B. Buck, Phys. Rev. **130**, 712 (1963).
[5] T. Tamura, Rev. Mod. Phys. **37**, 241 (1965).
[6] C. Mahaux and H. Ngô, Nucl. Phys. **A431**, 486 (1984).
[7] C. Mahaux, H. Ngô, and G. R. Satchler, Nucl. Phys. **A449**, 354 (1986).
[8] C. Mahaux and R. Sartor, Nucl. Phys. **A468**, 193 (1987).
[9] C. H. Johnson, D. J. Horen, and C. Mahaux, Phys. Rev. C **36**, 2252 (1987).
[10] C. Mahaux and R. Sartor, Nucl. Phys. **A484**, 205 (1988).
[11] C. Mahaux and R. Sartor, Nucl. Phys. **A493**, 157 (1989).
[12] R. W. Finlay, J. Wierzbicki, R. K. Das, and F. S. Dietrich, Phys. Rev. C **39**, 804 (1989).
[13] J. P. Delaroche, Y. Wang, and J. Rapaport, Phys. Rev. C **39**, 391 (1989).
[14] W. Tornow, Z. P. Chen, and J. P. Delaroche, Phys. Rev. C **42**, 693 (1990).
[15] C. Mahaux and R. Sartor, Nucl. Phys. **A528**, 253 (1991).
[16] C. Mahaux and R. Sartor, *Advances in Nuclear Physics*, edited by J. W. Negele and E. Vogt (Plenum, New York, 1991) Vol. 20.
[17] R. Lipperheide, Nucl. Phys. **A89**, 97 (1966).
[18] R. Lipperheide, Z. Phys. **202**, 58 (1967).
[19] G. Passatore, Nucl. Phys. **A95**, 694 (1967).
[20] R. Lipperheide and A. K. Schmidt, Nucl. Phys. **A112**, 65 (1968).
[21] A. Koning and J. P. Delaroche, Nucl. Phys. **A713**, 231 (2003).
[22] A. Koning, Private communication, 2000.
[23] B. Morillon and P. Romain, Phys. Rev. C **70**, 014601 (2004).
[24] P. Romain and J. P. Delaroche, A dispersive coupled channel analysis of nucleon scattering from ^{181}Ta and ^{182,184,186}W up to 200 MeV. In *Proceedings of the Meeting on Nucleon-Nucleus Optical Model up to 200 MeV, Bruyères-le-Châtel*, p. 167. Available online at http://www.nea.fr/html/science/om200/
[25] R. W. Finlay, W. P. Abfalterer, G. Fink, E. Montei, T. Adami, P. Lisowski, G. L. Morgan, and R. C. Haight, Phys. Rev. C **47**, 237 (1993).
[26] A. Molina, R. Capote, J. M. Quesada, and M. Lozano, Phys. Rev. C **65**, 034616 (2002).
[27] A. B. Smith, Ann. Nucl. Energy **31**, 1813 (2004).
[28] A. B. Smith, Ann. Nucl. Energy **29**, 1241 (2002).
[29] A. B. Smith, Ann. Nucl. Energy **28**, 1745 (2001).
[30] A. Trkov, Technical report **INDC(NDS)-447**, IAEA, Vienna, 2003. Available online at http://www-nds.iaea.org/reports/indc-nds-447.pdf

[31] C. H. Johnson and C. Mahaux, Phys. Rev. C **38**, 2589 (1988).
[32] A. M. Lane, Phys. Rev. Lett. **8**, 171 (1962).
[33] A. M. Lane, Nucl. Phys. **35**, 676 (1962).
[34] W. P. Abfalterer, F. B. Bateman, F. S. Dietrich, R. W. Finlay, R. C. Haight, and G. L. Morgan, Measurement of neutron total cross sections up to 560 MeV, Phys. Rev. C **63**, 044608 (2001).
[35] K. Volev, N. Koyumdjieva, A. Brusegan, A. Borella, P. Siegler, N. Janeva, A. Lukyanov, L. Leal and P. Schillebeeckx, Evaluation of the ^{232}Th neutron cross sections between 4 and 140 keV, AIP Conf. Proc. **769**, 87 (2005).
[36] Ch. Lagrange, Critique of nuclear models and their validity in the evaluation of nuclear data. In *Report NEANDC(J)-38 'L', INDC(JAP) 25/L 58*, 1975.
[37] E. Sh. Soukhovitskiĭ, S. Chiba, J-Y. Lee, O. Iwamoto, and T. Fukahori, J. Phys. G: Nucl. Part. Phys. **30**, 905 (2004).
[38] E. Sh. Soukhovitskiĭ, O. Iwamoto, S. Chiba, and T. Fukahori, J. Nucl. Sci. Technol. **37**, 120 (2000).
[39] R. H. Bassel, R. M. Drisko, and G. R. Satchler, Technical report **ORNL-3240**, Oak Ridge National Laboratory, 1962.
[40] S. Chiba, O. Iwamoto, Y. Yamanouti, M. Sugimoto, M. Mizumoto, K. Hasegawa, E. Sh. Soukhovitskiĭ, Y. V. Porodzinskiĭ, and Y. Watanabe, Nucl. Phys. **A624**, 305 (1997).
[41] L. R. B. Elton, Nuovo Cimento B **42**, 227 (1966).
[42] G. E. Brown and M. Rho, Nucl. Phys. **A372**, 397 (1981).
[43] C. Mahaux and R. Sartor, Nucl. Phys. **A458**, 25, 1986.
[44] J. M. VanderKam, G. J. Weisel, and W. Tornow, J. Phys. G: Nucl. Part. Phys. **26**, 1787 (2000).
[45] R. L. Walter, Analyzing power measurements and the nucleon-nucleus optical potential;a focus on the spin-orbit potential. In *Proceedings of the Meeting on Nucleon-Nucleus Optical Model up to 200 MeV, Bruyères-le-Châtel*, p. 199. Available online at http://www.nea.fr/html/science/om200/, OECD, Paris, 1997.
[46] J. M. Quesada, R. Capote, A. Molina, M. Lozano, and J. Raynal, Phys. Rev. C **67**, 067601 (2003).
[47] Cross Section Evaluation Working Group 1991 Report. Technical report **BNL-NCS-17541 (ENDF201)**, edited by P. F. Rose, National Nuclear Data Center, Brookhaven National Laboratory, Upton, NY, USA, 1991.
[48] V. McLane, C. L. Dunford, and P. F. Rose, *Neutron Cross Sections* (Academic Press, New York, 1988), Vol. 2.
[49] T. Iwasaki, M. Baba, K. Hattori, K. Kanda, S. Chiba, K. Kanoda, and N. Hirakawa, Measurements of neutron total cross section for Th-232 (EXFOR 21766). In *Contribution to the Specialists' Meeting on Fast Neutron Scattering on Actinide Nuclei*, Japan, 1981.
[50] W. P. Poenitz, J. F. Whalen, and A. B. Smith, Total neutron cross sections of heavy nuclei (EXFOR 10935), Nucl. Sci. Eng. **78**, 333 (1981).
[51] W. P. Poenitz, J. F. Whalen, Neutron total cross section measurements in the energy region from 47 keV to 20 MeV (EXFOR 12853). Technical report **ANL-NDM-80**, Argonne National Laboratory, USA, 1983.
[52] G. Haouat, J. Lachkar, Ch. Lagrange, J. Jary, J. Sigaud, and Y. Patin, neutron scattering cross sections for Th-232, U-233, U-235, U-238, Pu-239 AND Pu-242 between 0.6 AND 3.4 MeV (EXFOR 21782), Nucl. Sci. Eng. **81**, 491 (1982).
[53] A. B. Smith and S. Chiba, Ann. Nucl. Energy **23**, 459 (1996).
[54] R. Batchelor, W. B. Gilboy, and J. H. Towle, Neutron interactions with U-238 and Th-232 in the energy region 1.6 MeV to 7 MeV (EXFOR 21019), Nucl. Phys. **A65**, 236 (1965).
[55] T. Iwasaki, M. Baba, K. Hattori, K. Kanda, S. Chiba, K. Kanoda, and N. Hirakawa, A study of neutron scattering for Th-232 in MeV energy region (EXFOR 21767). In *Contribution to the Specialists' Meeting on Fast Neutron Scattering on Actinide Nuclei*, Japan, 1981.
[56] G. Dagge, W. Grum, J. W. Hammer, K.-W. Hoffmann, and G. Schreder, Optical model analysis over a wide range of nuclei using polarized neutron scattering data , Phys. Rev. C **39**, 1768 (1989).
[57] L. F. Hansen, B. A. Pohl, C. Wong, R. C. Haight, and Ch. Lagrange, Phys. Rev. C **34**, 2075 (1986).
[58] Ju. V. Dukarevich and A. N. Djumin, Elastic scattering of fast neutrons at small angles (EXFOR 40078) (in Russian), Zh. Eksp. Teor. Fiz. **44**, 130 (1961).
[59] C. I. Hudson, W. S. Walker, Jr., and S. Berko, Differential Elastic Scattering of 15.2-MeV Neutrons by Ta, Bi, Th, U (EXFOR 12180), Phys. Rev. **128**, 1271 (1962).
[60] L. F. Hansen, I. D. Proctor, D. W. Heikkinen, and V. A. Madsen, Nuclear deformation in the actinide region by proton inelastic scattering , Phys. Rev. C **25**, 189 (1982).
[61] C. H. King, J. E. Finck, G. M. Crawley, J. A. Nolen, Jr., and R. M. Ronningen, Multiple moments of 154Sm, 176Yb, 232Th, and 238U from proton inelastic scattering, Phys. Rev. C **20**, 2084 (1979).
[62] Y. Takeuchi, H. Sakaguchi, M. Nakamura, T. Ichihara, M. Yosoi, M. Ieiri, and S. Kobayashi, Quadrupole and hexadecapole moments of Th-232 and U-238 from inelastic scattering of 65 MeV polarized protons, Phys. Rev. C **34**, 493 (1986).
[63] H. Sakaguchi, Private communication, 2003.
[64] T. Belgya, O. Bersillon, R. Capote, T. Fukahori, G. Zhigang, S. Goriely, M. Herman, A. V. Ignatyuk, S. Kailas, A. Koning, P. Oblozhinsky, V. Plujko, and P. Young, *Handbook for calculations of nuclear reaction data: Reference Input Parameter Library*. Available online at http://www-nds.iaea.org/RIPL-2/, IAEA, Vienna, 2005.
[65] E. Sh. Soukhovitskiĭ, S. Chiba, O. Iwamoto, K. Shibata, T. Fukahori, and G. B. Morogovskiĭ, *Programs OPTMAN and SHEMMAN Version 8*. Technical report **JAERI-Data/Code 2005-002**, Japan Atomic Energy Research Institute, 2005.
[66] E. Sh. Soukhovitskiĭ, G. B. Morogovskiĭ, S. Chiba, O. Iwamoto, and T. Fukahori, *Physics and Numerical Methods of OPTMAN: A Coupled-channels Method Based on Soft-rotator Model for a Description of Collective Nuclear Structure and Excitation*. Technical report **JAERI-Data/Code 2004-002**, Japan Atomic Energy Research Institute, 2004.
[67] R. Capote, A. Molina, and J. M. Quesada, J. Phys. G: Nucl. Part. Phys. **27**, B15 (2001).
[68] J. M. Quesada, R. Capote, A. Molina, and M. Lozano, Comput. Phys. Commun. **153**, 97 (2003).
[69] E. Garrote, R. Capote, and R. Pedrosa, Comput. Phys. Commun. **92**, 267 (1995).
[70] C. B. Fulmer, Phys. Rev. **116**, 418 (1959).
[71] P. Kirkby and W. T. Link, Faraday-cup measurement of proton total reaction cross sections at 100 MeV (EXFOR O0340), Can. J. Phys. **44**, 1847 (1966).
[72] B. S. Varashenkov, *Cross sections of particle and nucleus interactions with nuclei* (in Russian). Technical report, Joint Institute for Nuclear Research, Dubna, Russia, 1993.
[73] K. Brueckner, C. Levinson, and H. Mahmoud, Phys. Rev. **95**, 217 (1954).
[74] F. Perey and B. Buck, Nucl. Phys. **32**, 353 (1962).

[75] G. E. Brown, J. Dehesa, and J. Speth, Nucl. Phys. **A330**, 389 (1979).
[76] C. Mahaux and H. Ngô, Phys. Lett. **B100**, 285 (1981).
[77] G. W. Greenlees, G. J. Pyle, and Y. C. Tang, Phys. Rev. **171**, 1115 (1968).
[78] G. W. Greenlees, G. J. Pyle, and Y. C. Tang, Phys. Lett. **B26**, 658 (1968).
[79] M. A. Nagarajan, C. C. Mahaux, and G. R. Satchler, Phys. Rev. Lett. **54**, 1136 (1985).
[80] M. Lozano, Phys. Rev. C **36**, 452 (1987).